JACS
JOURNAL OF THE AMERICAN CHEMICAL SOCIETY
pubs.acs.org/JACS
Article

Spatially Selective MicroRNA Imaging in Human Colorectal Cancer Tissues Using a Multivariate-Gated Signal Amplification Nanosensor

Xiaoming Zhang,[§] Wenhui Chen,[§] Songlin Wan,[§] Bing Qu, Fei Liao, Di Cheng, Yun Zhang, Zhao Ding,* Yanbing Yang,* and Quan Yuan*

Cite This: https://doi.org/10.1021/jacs.4c16001
Read Online

ABSTRACT: MicroRNA (miRNA) is involved in the genesis in viand development of colorectal cancer. The in vivo imaging of miRNA at the tumor sites is essential for understanding its role in colorectal cancer pathology and therapeutic target identification. However, achieving accurate imaging of miRNA at the tumor sites is hindered by the low abundance of miRNAs in tumor cells and nonspecific signal leakage in normal tissues. Here, we report a multivariate-gated catalytic hairpin assembly (CHA) nanosensor for the specific amplified imaging of microRNA-21 (miR-21) in human colorectal cancer tissues to reveal the underlying miR-21-associated molecular mechanism. The endogenous glutathione and exogenous near-infrared multivariate-gated design in combination with CHA probes improves the signal strength of target miR-21 and reduces the background interference. The nanosensor enables specific amplified imaging of miR-21 in vivo, and the signal-to-background ratios are 1.6-fold compared with traditional CHA methods. With the assistance of the designed nanosensor, we achieve the preliminary identification of tumor tissues and normal tissues from human clinical surgical resection samples. The overexpressed miR-21 is found to suppress the core mismatch repair recognition protein human mutS homologue 2 involved in DNA damage recognition and repair to inhibit the therapeutic efficacy of colorectal cancer. The strategy of probe design, which combines multivariate-gated activation methods with a signal amplification system, is applicable for accurate miRNA imaging and disease-relevant molecular mechanism research.

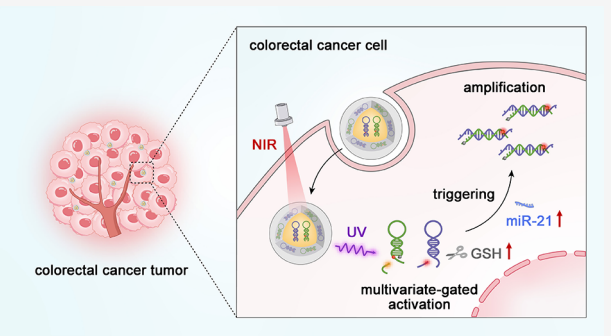

INTRODUCTION

As a common malignant tumor of the digestive system, colorectal cancer (CRC) has become one of the leading causes of cancer-related deaths and severely threatens human health.[1−3] MicroRNA (miRNA), a crucial endogenous gene regulator, is involved in numerous biological processes, and the abnormal expression of miRNA has been proven to be closely associated with low survival rate and distant metastatic development of CRC patients.[4−9] The high levels of microRNA-21 (miR-21) in CRC can down-regulate the expression of the core mismatch repair (MMR) protein human mutS homologue 2 (hMSH2), further causing a significant reduction of G2/M damage arrest and apoptosis induced by a chemotherapy drug 5-fluorouracil (5-FU), ultimately severely affecting the treatment efficiency of CRC patients.[10,11] In vivo miRNA imaging in CRC is thus a promising approach for understanding the genesis and development of tumors.[12−16] However, precise miRNA imaging is hindered by inadequate sensitivity, originating from the low abundance of miRNA targets in tumor regions and nonspecific signal leakage in normal tissues.

In the past few years, various signal amplification strategies capable of sensitive RNA detection have been developed.[14,17] Among them, enzyme-assisted signal amplification systems, such as rolling-circle amplification[18,19] and loop-mediated isothermal amplification,[20,21] afford the opportunity for RNA detection with high sensitivity, yet these systems are severely limited for application in vivo. Enzyme-free signal amplification systems, including hybridization chain reaction (HCR)[22−24] and catalytic hairpin assembly (CHA),[25−27] have been proposed for amplified RNA imaging in vitro and in vivo due to their simple and nonenzymatic processes.[28,29] However, the probes used in traditional enzyme-free signal amplification systems are constitutively in an activated state and generally triggered passively by targets before reaching the desired regions, leading to severe background signal interference and insufficient sensitivity in the specific imaging of RNA targets in body tissues. Moreover, the application of RNA imaging probes in

Received: November 12, 2024
Revised: January 19, 2025
Accepted: January 28, 2025

Scheme 1. Multivariate-Gated Specific Activation of Signal Amplification in miR-21 Imaging: (a) Schematic of the GSH/UV-Activated Amplification Mechanism of M-CHA Probes; and (b) Schematic of miR-21 Imaging with the M-CHA/U Nanosensor in Fresh Tissue Samples Derived from CRC Patients

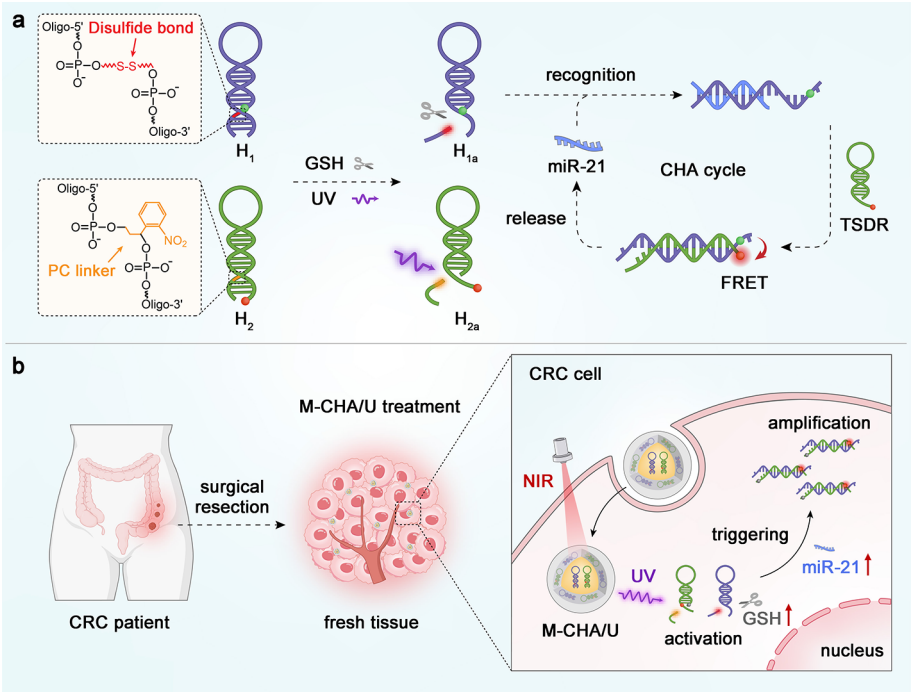

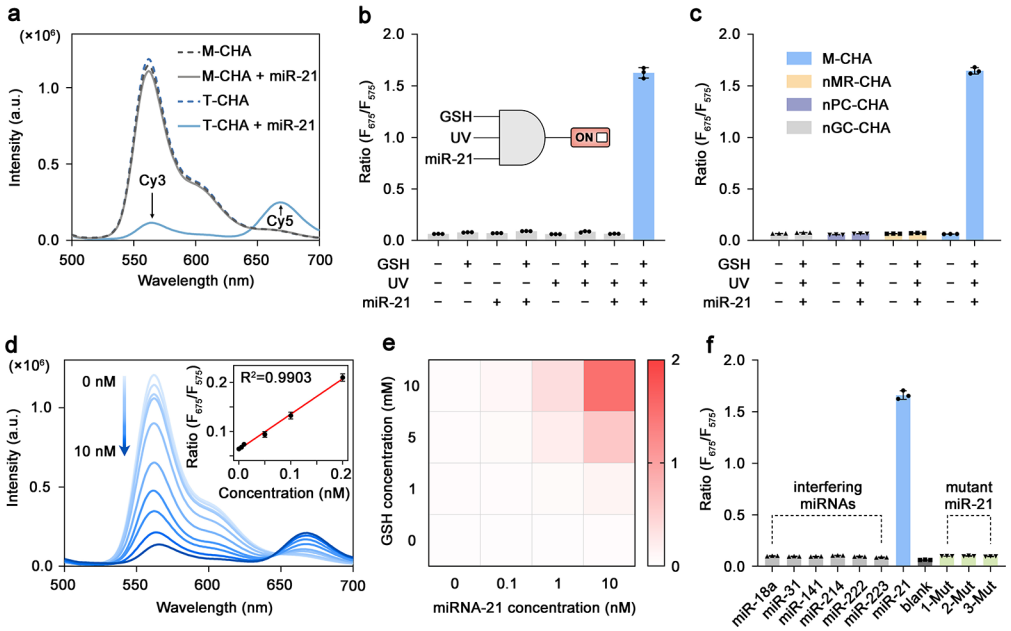

Figure 1. Evaluation of M-CHA for miR-21 detection in vitro. (a) Fluorescence spectra of the M-CHA and T-CHA responding to miR-21 (10 nM) without GSH and UV light. (b) Fluorescence ratio (F_{675}/F_{575}) of M-CHA with or without GSH (10 mM), UV light (365 nm, 5 mW/cm^2, 5 min), and miR-21 (10 nM) treatment. (c) Fluorescence ratio (F_{675}/F_{575}) of nGC−CHA, nPC−CHA, nMR-CHA, and M-CHA with or without GSH (10 mM), UV light (365 nm, 5 mW/cm^2, 5 min), and miR-21 (10 nM) treatment. (d) Fluorescence spectra of M-CHA responding to various concentrations of miR-21 (0−10 nM) with GSH (10 mM) and UV light (365 nm, 5 mW/cm^2, 5 min) activation. Inset: the plot of the fluorescence ratio (F_{675}/F_{575}) at different concentrations of miR-21. (e) Heat map analysis of M-CHA responding to various concentrations of miR-21 and GSH with UV light (365 nm, 5 mW/cm^2, 5 min) treatment. (f) Fluorescence ratio (F_{675}/F_{575}) of M-CHA responding to various RNAs (10 nM) with GSH (10 mM) and UV light (365 nm, 5 mW/cm^2, 5 min) activation. All reactions used 100 nM corresponding molecular beacons. Data presented as mean values ± SD, $n = 3$.

vivo often faces issues of enzymatic degradation in complex physiological environments and low cellular uptake efficiency due to the electrostatic membrane barrier.[29,30]

The inclusion of activation factors could trigger the selective signal amplification process in a spatiotemporally controllable way, thereby providing opportunities for high-sensitivity and high-specificity RNA imaging.[31−34] Inspired by the above

https://doi.org/10.1021/jacs.4c16001
J. Am. Chem. Soc. XXXX, XXX, XXX−XXX

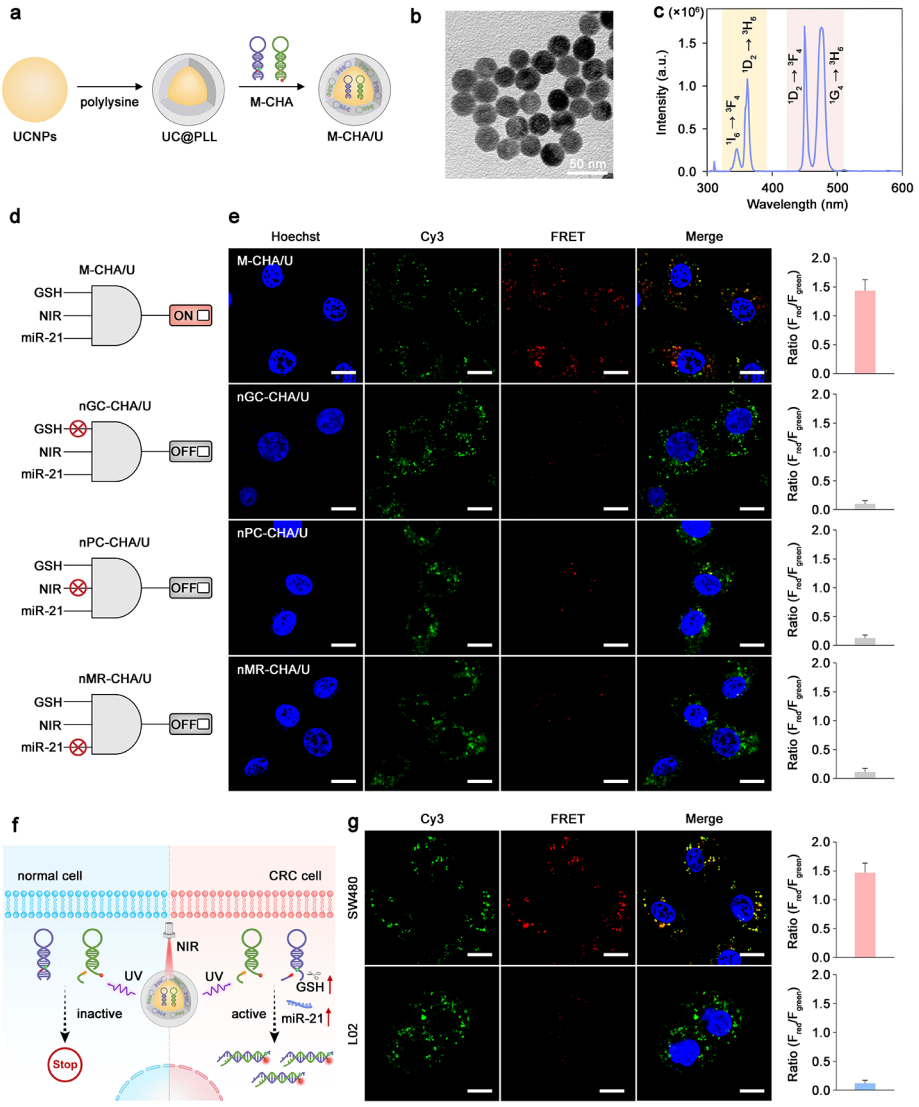

Figure 2. Multivariate-gated strategy for imaging of miR-21 in living cells. (a) Schematic illustration of the synthesis process of M-CHA/U. (b) TEM image of the M-CHA/U. (c) Emission spectra of M-CHA/U with 980 nm NIR laser irradiation. (d) Schematic illustration of the M-CHA/U, nGC−CHA/U, nPC−CHA/U, and nMR-CHA/U working mechanism. (e) CLSM images and corresponding quantification of the fluorescence intensity ratio (F_{red}/F_{green}) of SW480 cells treated with M-CHA/U, nGC−CHA/U, nPC−CHA/U, and nMR-CHA/U, respectively, followed by NIR laser irradiation. Scale bars: 10 μm. (f) Schematic illustration of M-CHA/U-mediated imaging of miR-21 in normal and CRC cells. (g) CLSM images and corresponding quantification of the fluorescence intensity ratio (F_{red}/F_{green}) of SW480 cells and L02 cells treated with M-CHA/U, followed by NIR laser irradiation. Scale bars: 10 μm. Data presented as mean values ± SD, n = 3.

considerations, we combined multivariate-gated catalytic hairpin assembly (M-CHA) probes with upconversion nanoparticles (UCNPs) to develop a multivariate-gated signal amplification nanosensor (M-CHA/U) for the specific amplified imaging of miRNA in human CRC tissues (Scheme 1). In our design, the activity of M-CHA probes is inhibited by the glutathione (GSH)-gated module and the light-gated module. Furthermore, UCNPs are employed as a light transducer and also serve as the delivery vehicle of M-CHA, which could effectively enhance the stability of imaging probes in physiological environments and facilitate intracellular delivery of the probes.[35,36] Based on the multivariate-gated signal amplification design, the nanosensor could be specifically triggered by endogenous GSH and exogenous near-infrared (NIR) light stimulation to achieve improved sensitivity and spatiotemporal precision for imaging of miR-21 in vivo. Benefiting from its robust imaging specificity and sensitivity, the nanosensor enables the amplified imaging of miR-21 in human CRC clinical histological samples, successfully achieving the preliminary identification of tumor tissues and normal tissues. By tracing miR-21 in CRC patients, we demonstrated that up-regulated miR-21 in CRC could inhibit the level of DNA MMR protein hMSH2, which may provide evidence for revealing the miR-21 relevant CRC molecular mechanism. The unique miRNA imaging design offers a strategy to assist in therapeutic target identification and to achieve the diagnosis and prognosis of cancer.

RESULTS AND DISCUSSION

Design and Evaluation of Multivariate-Gated M-CHA In Vitro. The multivariate-gated activating amplification mechanism of M-CHA is shown in Scheme 1 and Figure S1. In the M-CHA, the GSH-gated module and the light-gated module are designed through the incorporation of a disulfide

https://doi.org/10.1021/jacs.4c16001
J. Am. Chem. Soc. XXXX, XXX, XXX−XXX

bond and photocleavable (PC) linker into the hairpin stem of molecular beacon probes H_1 and H_2, respectively. The toehold regions in H_1 and H_2 are blocked in the stem regions to avoid undesired triggering. Upon stimulation with GSH and irradiation with ultraviolet (UV) light, the disulfide bond and the PC linker on H_1 and H_2 will be broken.[37−39] Due to the reduced binding affinity of H_1 and H_2, the 8-base single-stranded fragment will dissociate from H_1 and H_2 to yield H_{1a} and H_{2a} structures, thus exposing the toehold regions. The metastable probe H_{1a} can hybridize with target miR-21 to initiate a branch migration reaction and open the stem region. Subsequently, the cascade reaction between H_{1a} and H_{2a} will be triggered by toehold-mediated strand displacement reaction (TSDR) to generate an H_{1a}−H_{2a} pair, further releasing miR-21 to participate in the next round of the CHA cycle.[40] After numerous cycles, a certain amount of H_{1a}−H_{2a} pairs will be produced to achieve target signal amplification. When excited at a wavelength of 490 nm, each H_{1a}−H_{2a} pair could generate fluorescence resonance energy transfer (FRET) between Cy3 and Cy5 fluorophores which are labeled in H_{1a} and H_{2a}, respectively,[41,42] resulting in a "turn-on" fluorescence signal at 675 nm and a "turn-off" fluorescence signal at 575 nm to achieve high-sensitivity miR-21 imaging.

The feasibility of the M-CHA probes for miR-21 detection was first tested in an aqueous solution by FRET analysis. As shown in Figure 1a, the traditional persistently activated CHA probes (T-CHA) with the addition of miR-21 display a significant FRET signal, including Cy3 fluorescence decrease and Cy5 fluorescence increase. By contrast, M-CHA shows no obvious FRET signal in the presence of miR-21, indicating that the activity of CHA is inhibited by the designed multivariate-gated module. Also, the M-CHA shows a negligible FRET signal in the absence of any one of the three inputs (GSH, UV, and miR-21) (Figures 1b and S2). When exposed to miR-21, an obvious FRET signal is observed for the M-CHA upon activation with both GSH and UV, suggesting the initiation of the GSH/UV-controlled CHA process. The GSH and UV cospecific activation mechanism of the M-CHA was verified by polyacrylamide gel electrophoresis (PAGE) (Figure S3). After treatment of H_1 and H_2 with GSH and UV, respectively, a band of lower molecular weight appears (lanes 2 and 4), confirming the breaking of the disulfide bond and PC linker. Upon the addition of miR-21, the group of M-CHA with GSH and UV treatment shows a higher molecular weight band (lane 9), implying the specific activation of signal amplification. To further determine the origin of the FRET signal, as the control, we designed two systems with the same sequences as M-CHA but without disulfide bond within H_1 (nGC−CHA) and without PC linker within H_2 (nPC−CHA), respectively (Figure S4). The nGC−CHA and nPC−CHA show no obvious FRET signal in response to the target miR-21 under the stimulation of GSH and UV light (Figure 1c), indicating that the disulfide bond and PC linker are indispensable for the multivariate-gated activation probe design. As another negative control, nMR-CHA consisting of H_2 and H_{1m}, with several mutating bases in H_1, was designed (Figure S4). The nMR-CHA shows a negligible FRET signal in response to target miR-21 (Figure 1c), suggesting that the FRET signal in M-CHA is attributed to miR-21-induced CHA reaction.

After UV irradiation for 5 min, the FRET signal of M-CHA incubated with GSH and miR-21 increased continuously upon prolonged incubation time and reached a plateau at an incubation time of 180 min (Figure S5). Once the feasibility of M-CHA for specific activation was verified, we evaluated its performance for miR-21 detection. As depicted in Figures 1d and S6, the FRET signal of M-CHA shows a gradual enhancement with the concentration of miR-21 elevating, and the detection limit of M-CHA is calculated to be 10 pM. Furthermore, M-CHA exhibits a concentration-dependent FRET signal in response to both miR-21 and GSH (Figure 1e). Next, we introduced a series of interfering miRNA and base-mismatched miR-21 into M-CHA to investigate its selectivity and specificity. A negligible FRET signal induced by the interfering miRNA is observed, demonstrating the excellent selectivity of M-CHA for discerning target miR-21 (Figures 1f and S7). In addition, compared with the group of intact miR-21, no obvious FRET signal could be obtained for mutant miR-21 (Figures 1f and S8), indicating the specificity of M-CHA for distinguishing the base mutant target from the intact target. The GSH-based selective activation of M-CHA was further validated by replacing GSH in three inputs with other amino acids, showing that the FRET signal of GSH-controlled M-CHA is much higher than other amino acid groups (Figure S9).

Amplified Imaging of miR-21 in Living Cells. Considering the deep tissue penetration and low toxicity of NIR light, UCNPs that could transfer long-wavelength light to short-wavelength light were chosen as the NIR-to-UV converter for PC linker photolysis.[43−46] Additionally, UCNPs could serve as a vehicle for the delivery of M-CHA in vitro and in vivo (Figure 2a). The $NaGdF_4$: Yb, Tm@$NaGdF_4$ UCNPs with a core−shell structure were synthesized by a thermal decomposition method.[47] Transmission electron microscopy (TEM) images indicate uniform hexagonal UCNPs with an average size of ∼30 nm (Figure S10). Elemental mapping and energy-dispersive X-ray spectroscopy (EDS) line scan confirm the core−shell structure of UCNPs (Figures S11 and S12). The emission spectra of UCNPs indicate that the core−shell structure could significantly enhance the intensity of upconversion luminescence by preventing the surface-induced quenching effect (Figure S13). The UCNPs were sequentially coated with a layer of cationic polymer polylysine (PLL) and loaded with M-CHA to construct an M-CHA/U nanosensor through electrostatic interactions (Figure 2b). The zeta potential increases from 40.5 mV (UCNPs) to 51.1 mV (UC@PLL) and converts to −29.5 mV (M-CHA/U), indicating the sequential coating of PLL and M-CHA probes on UCNPs (Figure S14). The average hydrodynamic size of UCNPs gradually increases during the coating process (Figure S14). The loading percent of M-CHA is calculated to be ∼70% by fluorescence intensity quantification. Upon irradiation with NIR light (980 nm), M-CHA/U shows characteristic UV peaks (346 and 365 nm), which matches with the UV wavelength requirement of PC linker photolysis, indicating that the UCNPs could be used for the UV light-driven activation of M-CHA (Figure 2c). Furthermore, M-CHA/U activated in cell lysate exhibits similar specificity and sensitivity compared with M-CHA probes, suggesting the feasibility of using NIR light to initiate the nanosensor (Figure S15). Meanwhile, M-CHA/U exhibits comparable performance to previous RNA detection studies, suggesting its potential for extending its applicability to diverse diseases (Table S2).

The cellular uptake ability of M-CHA/U was investigated by confocal laser scanning microscopy (CLSM). SW480 cells, a CRC cell line with the high level of endogenous GSH and miR-21,[10,48] were incubated with M-CHA/U. As shown in Figure S16, with the incubation time increasing from 1 to 4 h, the M-CHA/U exhibits gradually enhanced fluorescence intensity,

https://doi.org/10.1021/jacs.4c16001
J. Am. Chem. Soc. XXXX, XXX, XXX−XXX

indicating that the effective cellular internalization of M-CHA was achieved by UCNPs. Moreover, the free M-CHA group shows no obvious fluorescence signal in the cytoplasm compared with the M-CHA/U group due to the electrostatic membrane barrier (Figure S17). The colocalization study indicates that M-CHA/U could escape from the endo/lysosomes, which is consistent with the reported endo/lysosome disruption of PLL (Figure S18).[49] Additionally, the cytotoxicity test reveals that M-CHA, UCNPs, and NIR light show negligible toxicity on cell viability (Figure S19).

After verifying the efficient cellular uptake of M-CHA/U, we investigated the performance of M-CHA/U for miR-21 imaging in living cells (Figure 2d). The SW480 cells with the M-CHA/U treatment and 980 nm NIR light irradiation show an obvious FRET signal (Figure 2e). Similarly, we treated SW480 cells with nGC−CHA/U (UC@PLL loaded with nGC−CHA) and nPC−CHA/U (UC@PLL loaded with nPC−CHA) under the same conditions (Figure 2d). As shown in Figure 2e, a negligible cellular FRET signal can be observed, suggesting that the GSH and NIR light are essential for the specific activation of miR-21 imaging. As another control, nMR-CHA/U (UC@PLL loaded with nMR-CHA) also reveals no obvious FRET signal (Figure 2d,e), suggesting that the intracellular FRET signal of M-CHA is attributed to the target miR-21 triggering instead of a nonspecific response. The intracellular FRET signal quantification is obtained by calculating the ratio of red channel (F_{red}) to green channel (F_{green}) fluorescence intensity. The statistical analysis of the fluorescence intensity ratio (F_{red}/F_{green}) corroborates the findings from CLSM images (Figure 2e). To confirm that the target miR-21 imaging in CRC cells indeed comes from the GSH and NIR light specific activation, we further investigated the miR-21 imaging capability of M-CHA/U in living cells under different input conditions. To simulate living cells with different intracellular states, 3-bromopyruvic acid (3-BP), a GSH inhibitor,[50] and miR-21 inhibitor were used for downregulating the levels of GSH and miR-21, respectively, and the results of regulation were verified by the GSH kit and qRT-PCR (Figure S20). As expected, the group of SW480 cells with NIR light irradiation and without inhibitor treatment exhibits an obvious intracellular FRET signal, while all other negative control groups show a negligible FRET signal (Figure S21). Quantification analysis of the intracellular fluorescence indicates that the FRET ratio of SW480 cells with NIR light irradiation is much higher than that of the cells treated with other control groups (Figure S21). These results demonstrate that M-CHA/U enables amplified imaging of target miR-21 in living cells through exogenous NIR light and endogenous biomolecules (GSH and miR-21) specific activation.

As the varied expression levels of GSH and miR-21 in different cells, we further evaluated the ability of M-CHA/U to distinguish target cells from other cells (Figure 2f). We chose L02 cells, a normal cell line with low expression profiles of endogenous GSH and miR-21,[51,52] as a negative control. As shown in Figure 2g, SW480 cells show a much higher FRET signal intensity than L02 cells after treatment with M-CHA/U and subsequent NIR light irradiation. By contrast, upon T-CHA/U (UC@PLL loaded with T-CHA) treatment, both SW480 and L02 cells show an obvious FRET signal, which can be attributed to the nonspecific triggering of T-CHA/U and background signal leakage (Figure S22). Together, these outcomes confirm the feasibility of M-CHA/U for target cell-selective imaging via specific activation.

Amplified Imaging of miR-21 In Vivo. Inspired by the excellent biocompatibility and imaging performance of M-CHA/U in vitro, we further evaluated the capability of M-CHA/U for the imaging of CRC in vivo. M-CHA probes were modified by a Cy5/BHQ3 pair to increase the penetration depth. The amplification performance assay reveals that M-CHA/U displays approximately 7-fold and 5-fold higher fluorescence signals in test tubes and cell imaging than the conventional unamplified molecular beacon (MB/U), respectively (Figure S23). In addition, the M-CHA/U modified with Cy5/BHQ3 exhibits equally superior specificity and sensitivity, which is attributed to the design of multivariate-gated activation and CHA signal amplification (Figure S24). The fluorescence assay demonstrates that M-CHA/U possesses great stability compared with free probes (Figure S25). Furthermore, the modification with Cy5/BHQ3 has negligible toxicity on cell viability (Figure S26). Together, these results confirm the applicability of M-CHA/U for in vivo miRNA imaging.

Next, we constructed a nude Balb/c mice model with xenograft SW480 tumor and intravenously injected with M-CHA/U and three negative controls, nGC−CHA/U, nPC−CHA/U, and nMR-CHA/U, respectively. The fluorescence images of mice were collected at different time points after probe injection for 2 h and irradiated with NIR light (Figure 3a). The results indicate that mice treated with M-CHA/U show an obvious sustained fluorescence enhancement at the tumor sites, whereas the mice injected with nGC−CHA/U, nPC−CHA/U, and nMR-CHA/U show negligible fluorescence intensity (Figure 3b,c). Quantitative analysis at the tumor region displays that, after 4 h postirradiation, the fluorescence intensity of M-CHA/U-treated mice is 2.1-fold, 1.8-fold, and 1.9-fold higher than that of mice treated with nGC−CHA/U, nPC−CHA/U, and nMR-CHA/U, respectively (Figure 3c). These results indicate that the multivariate-gated activation and target miRNA triggering ability of M-CHA/U generate a specific tumor fluorescence signal response. The mice were then euthanized and dissected. Ex vivo tissue imaging demonstrates a variable fluorescence intensity in the normal organs. Moreover, the fluorescence signal of the tumor in the M-CHA/U group is 2.3-fold, 2.2-fold, and 2.1-fold higher than that in the control groups treated with nGC-CHA/U, nPC-CHA/U, and nMR-CHA/U, respectively, indicating that the fluorescence signal is highly tumor-specific (Figure 3d,e). The histological analysis of the main organs indicates that M-CHA/U exhibits outstanding biocompatibility in vivo (Figure S27). These findings demonstrate that M-CHA/U is capable of the specific and sensitive imaging of miR-21 in vivo.

As we have indicated, specific miR-21 imaging in vivo using traditional CHA probes is hindered by the low signal-to-background ratios. As shown in Figure 3f, the normal tissue in T-CHA/U groups displays much higher fluorescence intensity compared with those in M-CHA/U groups, which can be attributed to the unspecific activation of CHA. After 4 h of injection, quantitative analysis of the fluorescence ratio of the tumor-to-normal region shows that the M-CHA/U groups exhibit 1.6-fold higher fluorescence intensity than the T-CHA/U groups (Figure 3g). Ex vivo imaging of the tumor and normal organs further confirms the high signal-to-background ratios of the M-CHA/U groups (Figure 3h). Together, these results indicate that the design of multivariate-gated activation in M-CHA/U provides a notable improvement of specificity for CRC imaging in vivo compared with that of the traditional CHA probes.

https://doi.org/10.1021/jacs.4c16001
J. Am. Chem. Soc. XXXX, XXX, XXX−XXX

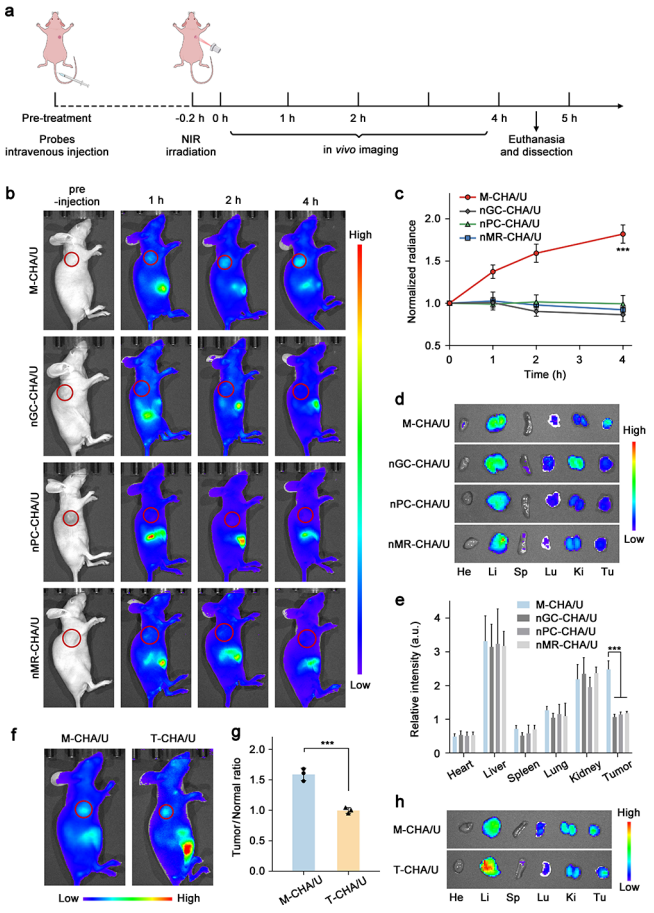

Figure 3. Multivariate-gated strategy for imaging miR-21 in vivo. (a) Illustration of M-CHA/U for miR-21 imaging through tail-vein injection. (b) Representative fluorescence imaging of SW480 tumor-bearing mice at different time points after treatment with M-CHA/U, nGC−CHA/U, nPC−CHA/U, and nMR-CHA/U, respectively. (c) Quantification analysis of tumor fluorescence signals of different groups in (b). (d) Ex vivo imaging and (e) corresponding quantification analysis of fluorescence intensity of tumor and major organs harvested from the mice with different probe treatments in (b). (f) Representative fluorescence imaging of SW480 tumor-bearing mice upon different probe treatments at 4 h postirradiation. (g) Ratio of fluorescence intensity of tumor to normal tissue of different groups in (f). (h) Ex vivo imaging of tumor and major organs harvested from the mice with different probe treatments in (f). He, Li, Sp, Lu, Ki, and Tu represent heart, liver, spleen, lung, kidney, and tumor, respectively. The red circles indicate the tumor regions. Data presented as mean values ± SD, $n = 3$. ***$P < 0.001$ (P values were determined by an unpaired two-sided t test or one-way ANOVA followed by Tukey's post hoc test).

Amplified Imaging of miR-21 in Clinical Surgical Samples. As a proof of concept, we investigated the feasibility of M-CHA/U for specific miR-21 imaging in CRC tissue samples. All of the samples were harvested from human patients who had undergone the surgical resection of CRC tumors. After surgical resection, the fresh tissue samples were immediately treated with M-CHA/U according to the procedures listed in Figure 4a and then imaged by a living imaging system. In each case, the tumor tissue and normal tissue in the images were taken from the same patient. As shown in Figure 4b, the fluorescence intensity of tumor tissues is much higher than that of normal tissues. Quantitative analysis of fluorescence intensity in tissue imaging and relative miR-21 expression of the corresponding tissues measured by qRT-PCR shows the same trend (Figures 4c and S28a). In addition, tumor tissues exhibit higher expression levels of GSH compared to normal tissues (Figure S28b). These results indicate that the fluorescence intensity of tissue imaging is positively correlated with the expression levels of GSH and miR-21, revealing that M-CHA/U may enable specific imaging of miR-21 in clinical CRC tissues. To further verify the discrimination capability of M-CHA/U, six representative CRC surgical resection specimens with adjacent normal tissues were harvested and treated using the same procedure as above. Significant differences in fluorescence intensity could be observed in each sample, reflecting the heterogeneity of miR-21 expression (Figure 4d). Two regions of interest (ROI) with obvious differences in fluorescence intensity were collected in each sample (Figure S29). Hematoxylin and eosin (H&E) staining of the selecting tissues indicates that the regions with higher fluorescence intensity exhibit a distinguishable cellular and structural atypia compared to the regions with lower fluorescence intensity, suggesting that miR-21 detection could serve as crucial means for CRC diagnosis (Figure 4e). Together, these outcomes demonstrate that the designed M-CHA/U nanosensor could effectively reveal the difference in miR-21 distribution in clinical tissues and distinguish tumor tissues from normal tissues. It is reported that the expression levels of miR-21 in tumor tissues are correlated with the stage of CRC, and more advanced tumors show higher expression levels.[53,54] Of note, the fluorescence intensity of the tumor exhibits a similar increasing trend with tumor progression, indicating the potential of the miRNA-biomarker imaging methods for differentiating different stages of cancer (Figure S30).

The high levels of miR-21 in CRC have been reported to directly target the 3′ untranslated region (UTR) of the hMSH2 mRNA in the MMR system, resulting in significant down-regulation of hMSH2 protein expression.[10] The hMSH2, a core MMR protein, plays an important role in DNA damage recognition and repair, and its absence would severely affect the course of treatment in CRC patients. Motivated by the performance of M-CHA/U in miR-21 imaging, we investigated the feasibility of M-CHA/U for investigating the miR-21-associated CRC molecular mechanism in clinical samples. The regions of tumor and normal tissues with obvious differences in fluorescence intensity after M-CHA/U treatment were selected, and the hMSH2 protein expression in these selected regions was analyzed by Western blotting and immunofluorescence imaging (Figures 4f,g and S31). The results indicate that the expression levels of hMSH2 protein in tissue regions with high fluorescence intensity are much lower than those in normal regions with no obvious fluorescence intensity. These outcomes suggest an inverse correlation between miR-21 and hMSH2 protein levels in CRC tissue, which is consistent with the reported conclusion that high levels of miR-21 would reduce the level of hMSH2 protein expression in CRC tumors. In brief, M-CHA/U with excellent sensitivity and specificity provides a promising tool for revealing the miRNA-associated disease molecular mechanism. Despite the progress made, several limitations should be taken into consideration in clinical applications. Cancer progression is associated with the abnormal expression of diverse biomarkers. Thus, developing multibiomarker-specific amplified imaging probes combined with the analysis of a large number of clinical samples in future research may offer the opportunities for more accurately identifying cancer characteristics, such as tumor stages and histological grading.[30,54,55]

https://doi.org/10.1021/jacs.4c16001
J. Am. Chem. Soc. XXXX, XXX, XXX−XXX

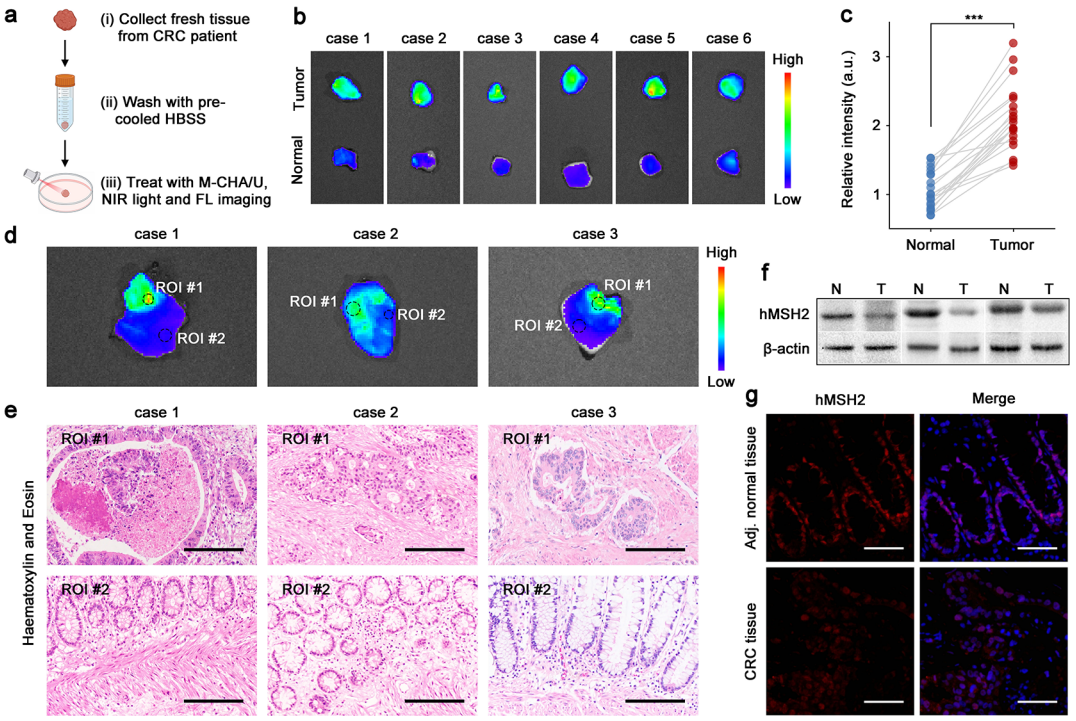

Figure 4. M-CHA/U application for imaging of CRC clinical surgical samples. (a) Procedures for clinical sample incubation and fluorescence imaging. (b) Fluorescence imaging of clinical tumor and normal tissue samples treated with M-CHA/U. (c) Relative fluorescence intensity of clinical tumor and normal tissue samples. ***$P < 0.001$ (P values were determined by a paired two-sided t test). (d) Fluorescence imaging of CRC clinical surgical samples with adjacent normal tissues treated with M-CHA/U. (e) Representative images of H&E staining regions of interest in (d). Scale bars: 100 μm. (f) Western blot analysis of relative expression levels of hMSH2 protein in tumor and adjacent normal tissues. (g) Immunofluorescence imaging of hMSH2 protein in tumor and adjacent normal tissues. Scale bars: 50 μm.

CONCLUSIONS

In conclusion, we designed a clinically applicable multivariable activation signal amplification M-CHA/U nanosensor for miR-21 imaging in human CRC tumor samples. The inclusion of multivariable activation in M-CHA/U enables signal amplification imaging of target miR-21 with high selectivity and sensitivity. The M-CHA/U shows superiority in specific amplified imaging of miR-21 with a high signal-to-background ratio in living CRC cells and in vivo. Based on the excellent miR-21 imaging performance, M-CHA/U also achieves the specific amplified imaging of miR-21 in clinical CRC tissue samples and distinguishes tumor tissues from normal tissues. With M-CHA/U, the overexpressed miR-21 in CRC tissue samples was found to have an inverse correlation with hMSH2 protein levels. The designed multivariable activation of the miRNA imaging strategy provides an option for disease-relevant biomolecule analysis technology, which is important for cancer diagnosis and treatment.

ASSOCIATED CONTENT

Supporting Information

The Supporting Information is available free of charge at https://pubs.acs.org/doi/10.1021/jacs.4c16001.

Time-dependent CLSM images of SW480 cells treated with M-CHA/U and NIR irradiation (MP4)

Materials and reagents, experimental details, DNA sequences used in this study, fluorescence analysis and gel electrophoresis of M-CHA probes, preparation and characterization of UCNPs, results of CLSM imaging, flow cytometric analysis, cell viability and biocompatibility analysis, and qRT-PCR experiments (PDF)

AUTHOR INFORMATION

Corresponding Authors

Zhao Ding − *College of Chemistry and Molecular Sciences, Department of Colorectal and Anal Surgery of Zhongnan Hospital of Wuhan University, Clinical Center of Intestinal and Colorectal Diseases of Hubei Province, Institute of Molecular Medicine, Renmin Hospital of Wuhan University, School of Microelectronics, Wuhan University, Wuhan 430072, P. R. China*; Email: dingzhao@whu.edu.cn

Yanbing Yang − *College of Chemistry and Molecular Sciences, Department of Colorectal and Anal Surgery of Zhongnan Hospital of Wuhan University, Clinical Center of Intestinal and Colorectal Diseases of Hubei Province, Institute of Molecular Medicine, Renmin Hospital of Wuhan University, School of Microelectronics, Wuhan University, Wuhan 430072, P. R. China*; Email: yangyanbing@whu.edu.cn

Quan Yuan − *College of Chemistry and Molecular Sciences, Department of Colorectal and Anal Surgery of Zhongnan Hospital of Wuhan University, Clinical Center of Intestinal and Colorectal Diseases of Hubei Province, Institute of Molecular Medicine, Renmin Hospital of Wuhan University, School of Microelectronics, Wuhan University, Wuhan 430072, P. R. China; Molecular Science and Biomedicine Laboratory (MBL), State Key Laboratory of Chemo/Biosensing and Chemometrics, College of Chemistry and Chemical Engineering, Hunan University, Changsha 410082, P. R. China*; orcid.org/0000-0002-3085-431X; Email: yuanquan@whu.edu.cn

https://doi.org/10.1021/jacs.4c16001
J. Am. Chem. Soc. XXXX, XXX, XXX−XXX

Authors

Xiaoming Zhang − *College of Chemistry and Molecular Sciences, Department of Colorectal and Anal Surgery of Zhongnan Hospital of Wuhan University, Clinical Center of Intestinal and Colorectal Diseases of Hubei Province, Institute of Molecular Medicine, Renmin Hospital of Wuhan University, School of Microelectronics, Wuhan University, Wuhan 430072, P. R. China*

Wenhui Chen − *College of Chemistry and Molecular Sciences, Department of Colorectal and Anal Surgery of Zhongnan Hospital of Wuhan University, Clinical Center of Intestinal and Colorectal Diseases of Hubei Province, Institute of Molecular Medicine, Renmin Hospital of Wuhan University, School of Microelectronics, Wuhan University, Wuhan 430072, P. R. China*

Songlin Wan − *College of Chemistry and Molecular Sciences, Department of Colorectal and Anal Surgery of Zhongnan Hospital of Wuhan University, Clinical Center of Intestinal and Colorectal Diseases of Hubei Province, Institute of Molecular Medicine, Renmin Hospital of Wuhan University, School of Microelectronics, Wuhan University, Wuhan 430072, P. R. China*

Bing Qu − *College of Chemistry and Molecular Sciences, Department of Colorectal and Anal Surgery of Zhongnan Hospital of Wuhan University, Clinical Center of Intestinal and Colorectal Diseases of Hubei Province, Institute of Molecular Medicine, Renmin Hospital of Wuhan University, School of Microelectronics, Wuhan University, Wuhan 430072, P. R. China*

Fei Liao − *College of Chemistry and Molecular Sciences, Department of Colorectal and Anal Surgery of Zhongnan Hospital of Wuhan University, Clinical Center of Intestinal and Colorectal Diseases of Hubei Province, Institute of Molecular Medicine, Renmin Hospital of Wuhan University, School of Microelectronics, Wuhan University, Wuhan 430072, P. R. China*

Di Cheng − *College of Chemistry and Molecular Sciences, Department of Colorectal and Anal Surgery of Zhongnan Hospital of Wuhan University, Clinical Center of Intestinal and Colorectal Diseases of Hubei Province, Institute of Molecular Medicine, Renmin Hospital of Wuhan University, School of Microelectronics, Wuhan University, Wuhan 430072, P. R. China*

Yun Zhang − *College of Chemistry and Molecular Sciences, Department of Colorectal and Anal Surgery of Zhongnan Hospital of Wuhan University, Clinical Center of Intestinal and Colorectal Diseases of Hubei Province, Institute of Molecular Medicine, Renmin Hospital of Wuhan University, School of Microelectronics, Wuhan University, Wuhan 430072, P. R. China*

Complete contact information is available at: https://pubs.acs.org/10.1021/jacs.4c16001

Author Contributions

[§]X.Z., W.C., and S.W. contributed equally to this work.

Notes

The authors declare no competing financial interest.

■ ACKNOWLEDGMENTS

The National Natural Science Foundation of China (21925401, 22322408, 22474096, and 52221001), the National Key R&D Program of China (2023YFF1205900 and 2021YFA1202400), the Fundamental Research Funds for the Central Universities (2042022rc0004 and 2042024kf1015), the Research Funds from the State Key Laboratory of Chemo/Biosensing and Chemometrics of Hunan University (20230755), the Hunan Provincial Key Research and Development Plan (2024JK2117), the New Cornerstone Science Foundation through the Xplorer Prize, and the "Sharp Knife" Technology Research Program of Hubei Province (2023BAA002) are acknowledged for research funding. We also thank the Core Facility of Wuhan University for TEM and FL spectra analysis.

■ REFERENCES

(1) Siegel, R. L.; Wagle, N. S.; Cercek, A.; Smith, R. A.; Jemal, A. Colorectal Cancer Statistics, 2023. *CA-Cancer J. Clin.* **2023**, *73*, 233−254.

(2) Hu, Z.; Ding, J.; Ma, Z.; Sun, R.; Seoane, J. A.; Scott Shaffer, J.; Suarez, C. J.; Berghoff, A. S.; Cremolini, C.; Falcone, A.; Loupakis, F.; Birner, P.; Preusser, M.; Lenz, H.-J.; Curtis, C. Quantitative Evidence for Early Metastatic Seeding in Colorectal Cancer. *Nat. Genet.* **2019**, *51*, 1113−1122.

(3) Center, M. M.; Jemal, A.; Smith, R. A.; Ward, E. Worldwide Variations in Colorectal Cancer. *CA-Cancer J. Clin.* **2009**, *59*, 366−378.

(4) Okugawa, Y.; Grady, W. M.; Goel, A. Epigenetic Alterations in Colorectal Cancer: Emerging Biomarkers. *Gastroenterology* **2015**, *149*, 1204−1225.e12.

(5) Ebert, M. S.; Sharp, P. A. Roles for MicroRNAs in Conferring Robustness to Biological Processes. *Cell* **2012**, *149*, 515−524.

(6) Calin, G. A.; Croce, C. M. MicroRNA Signatures in Human Cancers. *Nat. Rev. Cancer* **2006**, *6*, 857−866.

(7) Li, J.; Tan, S.; Kooger, R.; Zhang, C.; Zhang, Y. MicroRNAs as Novel Biological Targets for Detection and Regulation. *Chem. Soc. Rev.* **2014**, *43*, 506−517.

(8) Esteller, M. Non-Coding RNAs in Human Disease. *Nat. Rev. Genet.* **2011**, *12*, 861−874.

(9) Jung, G.; Hernández-Illán, E.; Moreira, L.; Balaguer, F.; Goel, A. Epigenetics of Colorectal Cancer: Biomarker and Therapeutic Potential. *Nat. Rev. Gastroenterol. Hepatol.* **2020**, *17*, 111−130.

(10) Valeri, N.; Gasparini, P.; Braconi, C.; Paone, A.; Lovat, F.; Fabbri, M.; Sumani, K. M.; Alder, H.; Amadori, D.; Patel, T.; Nuovo, G. J.; Fishel, R.; Croce, C. M. MicroRNA-21 Induces Resistance to 5-Fluorouracil by Down-Regulating Human DNA Muts Homolog 2 (hMSH2). *Proc. Natl. Acad. Sci. U.S.A.* **2010**, *107*, 21098−21103.

(11) Longley, D. B.; Harkin, D. P.; Johnston, P. G. 5-Fluorouracil: Mechanisms of Action and Clinical Strategies. *Nat. Rev. Cancer* **2003**, *3*, 330−338.

(12) Harvey, J. D.; Jena, P. V.; Baker, H. A.; Zerze, G. H.; Williams, R. M.; Galassi, T. V.; Roxbury, D.; Mittal, J.; Heller, D. A. A Carbon Nanotube Reporter of MicroRNA Hybridization Events in Vivo. *Nat. Biomed. Eng.* **2017**, *1*, 0041.

(13) Cheglakov, Z.; Cronin, T. M.; He, C.; Weizmann, Y. Live Cell MicroRNA Imaging Using Cascade Hybridization Reaction. *J. Am. Chem. Soc.* **2015**, *137*, 6116−6119.

(14) Le, P.; Ahmed, N.; Yeo, G. W. Illuminating RNA Biology through Imaging. *Nat. Cell Biol.* **2022**, *24*, 815−824.

(15) Wu, L.; Wang, Y.; Xu, X.; Liu, Y.; Lin, B.; Zhang, M.; Zhang, J.; Wan, S.; Yang, C.; Tan, W. Aptamer-Based Detection of Circulating Targets for Precision Medicine. *Chem. Rev.* **2021**, *121*, 12035−12105.

(16) Zhang, H.; Li, F.; Dever, B.; Li, X.; Le, X. C. DNA-Mediated Homogeneous Binding Assays for Nucleic Acids and Proteins. *Chem. Rev.* **2013**, *113*, 2812−2841.

(17) Wang, K.; Tang, Z.; Yang, C. J.; Kim, Y.; Fang, X.; Li, W.; Wu, Y.; Medley, C. D.; Cao, Z.; Li, J.; Colon, P.; Lin, H.; Tan, W. Molecular Engineering of DNA: Molecular Beacons. *Angew. Chem., Int. Ed.* **2009**, *48*, 856−870.

(18) Zhao, W.; Ali, M. M.; Brook, M. A.; Li, Y. Rolling Circle Amplification: Applications in Nanotechnology and Biodetection with Functional Nucleic Acids. *Angew. Chem., Int. Ed.* **2008**, *47*, 6330−6337.

(19) Lizardi, P. M.; Huang, X.; Zhu, Z.; Bray-Ward, P.; Thomas, D. C.; Ward, D. C. Mutation Detection and Single-Molecule Counting Using Isothermal Rolling-Circle Amplification. *Nat. Genet.* **1998**, *19*, 225−232.
(20) Zhao, Y.; Chen, F.; Li, Q.; Wang, L.; Fan, C. Isothermal Amplification of Nucleic Acids. *Chem. Rev.* **2015**, *115*, 12491−12545.
(21) Deng, R.; Zhang, K.; Li, J. Isothermal Amplification for MicroRNA Detection: From the Test Tube to the Cell. *Acc. Chem. Res.* **2017**, *50*, 1059−1068.
(22) Dirks, R. M.; Pierce, N. A. Triggered Amplification by Hybridization Chain Reaction. *Proc. Natl. Acad. Sci. U.S.A.* **2004**, *101*, 15275−15278.
(23) Wu, Z.; Liu, G.-Q.; Yang, X.; Jiang, J. Electrostatic Nucleic Acid Nanoassembly Enables Hybridization Chain Reaction in Living Cells for Ultrasensitive mRNA Imaging. *J. Am. Chem. Soc.* **2015**, *137*, 6829−6836.
(24) Choi, H. M. T.; Chang, J. Y.; Trinh, L. A.; Padilla, J. E.; Fraser, S. E.; Pierce, N. A. Programmable in Situ Amplification for Multiplexed Imaging of mRNA Expression. *Nat. Biotechnol.* **2010**, *28*, 1208−1212.
(25) Yin, P.; Choi, H. M. T.; Calvert, C. R.; Pierce, N. A. Programming Biomolecular Self-Assembly Pathways. *Nature* **2008**, *451*, 318−322.
(26) Wu, C.; Cansiz, S.; Zhang, L.; Teng, I. T.; Qiu, L.; Li, J.; Liu, Y.; Zhou, C.; Hu, R.; Zhang, T.; Cui, C.; Cui, L.; Tan, W. A Nonenzymatic Hairpin DNA Cascade Reaction Provides High Signal Gain of mRNA Imaging inside Live Cells. *J. Am. Chem. Soc.* **2015**, *137*, 4900−4903.
(27) Liu, J.; Zhang, Y.; Xie, H.; Zhao, L.; Zheng, L.; Ye, H. Applications of Catalytic Hairpin Assembly Reaction in Biosensing. *Small* **2019**, *15*, No. 1902989.
(28) Wang, W.; Ge, Q.; Zhao, X. Enzyme-Free Isothermal Amplification Strategy for the Detection of Tumor-Associated Biomarkers: A Review. *TrAC, Trends Anal. Chem.* **2023**, *160*, No. 116960.
(29) Qing, Z.; Xu, J.; Hu, J.; Zheng, J.; He, L.; Zou, Z.; Yang, S.; Tan, W.; Yang, R. In Situ Amplification-Based Imaging of RNA in Living Cells. *Angew. Chem., Int. Ed.* **2019**, *58*, 11574−11585.
(30) Xia, Y.; Zhang, R.; Wang, Z.; Tian, J.; Chen, X. Recent Advances in High-Performance Fluorescent and Bioluminescent RNA Imaging Probes. *Chem. Soc. Rev.* **2017**, *46*, 2824−2843.
(31) Liu, Q.; Huang, Y.; Li, Z.; Li, L.; Zhao, Y.; Li, M. An Enzymatically Gated Catalytic Hairpin Assembly Delivered by Lipid Nanoparticles for the Tumor-Specific Activation of Signal Amplification in miRNA Imaging. *Angew. Chem., Int. Ed.* **2022**, *61*, No. e202214230.
(32) He, Y.; Wang, Q.; Hong, C.; Li, R.; Shang, J.; Yu, S.; Liu, X.; Wang, F. A Smart Deoxyribozyme-Programmable Catalytic DNA Circuit for High-Contrast MicroRNA Imaging. *Angew. Chem., Int. Ed.* **2023**, *62*, No. e202307418.
(33) Sheng, C.; Zhao, J.; Di, Z.; Huang, Y.; Zhao, Y.; Li, L. Spatially Resolved in Vivo Imaging of Inflammation-Associated mRNA via Enzymatic Fluorescence Amplification in a Molecular Beacon. *Nat. Biomed. Eng.* **2022**, *6*, 1074−1084.
(34) Chu, H.; Zhao, J.; Mi, Y.; Zhao, Y.; Li, L. Near-Infrared Light-Initiated Hybridization Chain Reaction for Spatially and Temporally Resolved Signal Amplification. *Angew. Chem., Int. Ed.* **2019**, *58*, 14877−14881.
(35) Zhang, Y.; Zhang, Y.; Song, G.; He, Y.; Zhang, X.; Liu, Y.; Ju, H. A DNA−Azobenzene Nanopump Fueled by Upconversion Luminescence for Controllable Intracellular Drug Release. *Angew. Chem., Int. Ed.* **2019**, *58*, 18207−18211.
(36) Dong, H.; Du, S.; Zheng, X.; Lyu, G.; Sun, L.; Li, L.-D.; Zhang, P.; Zhang, C.; Yan, C. Lanthanide Nanoparticles: From Design toward Bioimaging and Therapy. *Chem. Rev.* **2015**, *115*, 10725−10815.
(37) Lee, M. H.; Yang, Z.; Lim, C. W.; Lee, Y. H.; Dongbang, S.; Kang, C.; Kim, J. S. Disulfide-Cleavage-Triggered Chemosensors and Their Biological Applications. *Chem. Rev.* **2013**, *113*, 5071−5109.
(38) Qiu, L.; Wu, C.; You, M.; Han, D.; Chen, T.; Zhu, G.; Jiang, J.; Yu, R.; Tan, W. A Targeted, Self-Delivered, and Photocontrolled Molecular Beacon for mRNA Detection in Living Cells. *J. Am. Chem. Soc.* **2013**, *135*, 12952−12955.
(39) Zheng, J.; Yang, R.; Shi, M.; Wu, C.; Fang, X.; Li, Y.; Li, J.; Tan, W. Rationally Designed Molecular Beacons for Bioanalytical and Biomedical Applications. *Chem. Soc. Rev.* **2015**, *44*, 3036−3055.
(40) Simmel, F. C.; Yurke, B.; Singh, H. R. Principles and Applications of Nucleic Acid Strand Displacement Reactions. *Chem. Rev.* **2019**, *119*, 6326−6369.
(41) Kikuchi, K. Design, Synthesis and Biological Application of Chemical Probes for Bio-Imaging. *Chem. Soc. Rev.* **2010**, *39*, 2048−2053.
(42) Ha, T.; Fei, J.; Schmid, S.; Lee, N. K.; Gonzalez, R. L.; Paul, S.; Yeou, S. Fluorescence Resonance Energy Transfer at the Single-Molecule Level. *Nat. Rev. Methods Primers* **2024**, *4*, 21.
(43) Fan, Y.; Wang, P.; Lu, Y.; Wang, R.; Zhou, L.; Zheng, X.; Li, X.; Piper, J. A.; Zhang, F. Lifetime-Engineered NIR-II Nanoparticles Unlock Multiplexed in Vivo Imaging. *Nat. Nanotechnol.* **2018**, *13*, 941−946.
(44) Hu, Z.; Fang, C.; Li, B.; Zhang, Z.; Cao, C.; Cai, M.; Su, S.; Sun, X.; Shi, X.; Li, C.; Zhou, T.; Zhang, Y.; Chi, C.; He, P.; Xia, X.; Chen, Y.; Gambhir, S. S.; Cheng, Z.; Tian, J. First-in-Human Liver-Tumour Surgery Guided by Multispectral Fluorescence Imaging in the Visible and Near-Infrared-I/II Windows. *Nat. Biomed. Eng.* **2020**, *4*, 259−271.
(45) Prodi, L.; Rampazzo, E.; Rastrelli, F.; Speghini, A.; Zaccheroni, N. Imaging Agents Based on Lanthanide Doped Nanoparticles. *Chem. Soc. Rev.* **2015**, *44*, 4922−4952.
(46) Cheng, X.; Zhou, J.; Yue, J.; Wei, Y.; Gao, C.; Xie, X.; Huang, L. Recent Development in Sensitizers for Lanthanide-Doped Upconversion Luminescence. *Chem. Rev.* **2022**, *122*, 15998−16050.
(47) Mai, H.; Zhang, Y.; Si, R.; Yan, Z.; Sun, L.; You, L.-P.; Yan, C. High-Quality Sodium Rare-Earth Fluoride Nanocrystals: Controlled Synthesis and Optical Properties. *J. Am. Chem. Soc.* **2006**, *128*, 6426−6436.
(48) Guo, R.; Huang, F.; Zhang, B.; Yan, Y.; Che, J.; Jin, Y.; Zhuang, Y.; Dong, R.; Li, Y.; Tan, B.; Song, R.; Hu, Y.; Dong, X.; Li, X.; Lin, N. GSH Activated Biotin-Tagged Near-Infrared Probe for Efficient Cancer Imaging. *Theranostics* **2019**, *9*, 3515−3525.
(49) Vaughan, H. J.; Green, J. J.; Tzeng, S. Y. Cancer-Targeting Nanoparticles for Combinatorial Nucleic Acid Delivery. *Adv. Mater.* **2020**, *32*, No. 1901081.
(50) Kwiatkowska, E.; Wojtala, M.; Gajewska, A.; Soszyński, M.; Bartosz, G.; Sadowska-Bartosz, I. Effect of 3-Bromopyruvate Acid on the Redox Equilibrium in Non-Invasive MCF-7 and Invasive MDA-MB-231 Breast Cancer Cells. *J. Bioenerg. Biomembr.* **2016**, *48*, 23−32.
(51) Li, L.; Wang, X.; Li, Q.; Liu, P.; Xu, K.; Chen, H.; Tang, B. An Accurate Mass Spectrometric Approach for the Simultaneous Comparison of GSH, Cys, and Hcy in L02 Cells and HepG2 Cells using New NPSP Isotope Probes. *Chem. Commun.* **2015**, *51*, 11317−11320.
(52) Ying, Z.; Wu, Z.; Tu, B.; Tan, W.; Jiang, J. Genetically Encoded Fluorescent RNA Sensor for Ratiometric Imaging of MicroRNA in Living Tumor Cells. *J. Am. Chem. Soc.* **2017**, *139*, 9779−9782.
(53) Schetter, A. J.; Leung, S. Y.; Sohn, J. J.; Zanetti, K. A.; Bowman, E. D.; Yanaihara, N.; Yuen, S. T.; Chan, T. L.; Kwong, D. L. W.; Au, G. K. H.; Liu, C.-G.; Calin, G. A.; Croce, C. M.; Harris, C. C. MicroRNA Expression Profiles Associated with Prognosis and Therapeutic Outcome in Colon Adenocarcinoma. *JAMA* **2008**, *299*, 425−436.
(54) Pardini, B.; Ferrero, G.; Tarallo, S.; Gallo, G.; Francavilla, A.; Licheri, N.; Trompetto, M.; Clerico, G.; Senore, C.; Peyre, S.; Vymetalkova, V.; Vodickova, L.; Liska, V.; Vycital, O.; Levy, M.; Macinga, P.; Hucl, T.; Budinska, E.; Vodicka, P.; Cordero, F.; Naccarati, A. A Fecal MicroRNA Signature by Small RNA Sequencing Accurately Distinguishes Colorectal Cancers: Results from a Multicenter Study. *Gastroenterology* **2023**, *165*, 582−599.e8.
(55) He, X.-P.; Hu, X.-L.; James, T. D.; Yoon, J.; Tian, H. Multiplexed Photoluminescent Sensors: Towards Improved Disease Diagnostics. *Chem. Soc. Rev.* **2017**, *46*, 6687−6696.

https://doi.org/10.1021/jacs.4c16001
J. Am. Chem. Soc. XXXX, XXX, XXX−XXX